A RANS INVESTIGATION OF WIND TUNNEL INTERFERENCE EFFECTS ON DELTA WING AERODYNAMICS

M. R. Allan*, K. J. Badcock†, G. N. Barakos‡, and B. E. Richards§

Computational Fluid Dynamics Lab,

Department of Aerospace Engineering,

University of Glasgow,

Scotland G12 8QQ, United Kingdom.

Tel. : +44(0)141 330 4106, Fax. : +44(0)141 330 5560, Email : mallan@aero.gla.ac.uk

Keywords: CFD, Delta Wing, Tunnel Interference, Vortex Breakdown

RANS simulations of a pitching delta wing within three wind tunnels have been performed, in order to ascertain the various influences tunnel walls have on delta wing aerodynamics. The presence of the tunnel walls has been found to promote vortex breakdown, with side wall proximity being the dominant factor. Roof and floor proximity are seen to have a negligible effect on vortex breakdown. During pitching motion, side wall proximity delays the reformation of the vortex after breakdown has reached its most upstream location, during cyclic pitching motion. This delay is recovered on the upstroke of the motion. Tunnel blockage does not appear to have a large effect on vortex breakdown. These results confirm previous work with Euler simulations of tunnel interference.

NOMENCLATURE

S/W	Wing span (S) to tunnel width (W)
S/H	Wing span (S) to tunnel height (H)
$\alpha(t)$	Instantaneous angle of attack
α_m	Mean angle of attack
α_0	Amplitude of pitching motion
k	Reduced frequency of pitching motion
t	Non-dimensional time
c_r	Root chord
C_L	Lift coefficient
C_D	Drag coefficient
η	Spanwise distance/local span
ω	Vorticity vector ($\nabla \times U$)

*Research Assistant, Member AIAA.

†Senior Lecturer.

‡Lecturer.

§Mechan Professor, Associate Fellow AIAA.

INTRODUCTION

WIND tunnels are used to test the aerodynamic characteristics of aircraft in the research and development stages. However, the influence of the tunnel walls must be taken into account when considering test results. Historically, wind tunnel corrections have been based on Linear Potential Flow Theory.[1] To obtain good quality and reliable test data, factors relating to wall interference, flow angularity, local variations in velocity, and support interference, must be taken into account. Karou[2] found that for delta wings with aspect ratio equal to one and spanning up to half the tunnel width, classical wall correction techniques can be used to correct flow field and force results up to 30^o angle of attack (it should be noted that vortex breakdown was unlikely to be present over the wing). Also, for swept wings with a blockage ratio (ratio of model planform area to tunnel cross-sectional area) of less than 0.08, tunnel interference effects can usually be considered negligible.[3]

Clearly, the flow conditions within a wind tunnel will be different to those a wing would experience in free air. The interactions between the wing and wall flow fields induce longitudinal and lateral variations (streamline curvature and aerodynamic twist respectively) to the freestream, in addition to those attributed to the wing alone. These differences may result in a reduction in the average downwash experienced by the model, a change in the streamline curvature about the model, an alteration to the local angle of attack along the span of the model, a change in dynamic pressure about the model due to solid and wake blockage, and in the buoyancy effect due to the axial pressure gradient along the tunnel test section. The magnitude of these effects increases

with model size (increasing solid blockage).

Weinberg[4] conducted an experimental investigation into wall effects. He tested two sets of three wings (one set with 60^o sweep, and one set with 70^o sweep), each wing with a different span size. The experiment was performed in a square water tunnel (low Re) at a constant flow velocity of 11m/s. The tunnel size was 45cm x 45cm. He found that for the three wings with 70^o sweep, as the wing size was increased (kept at a constant angle of attack), vortex breakdown moved downstream. For the three wings with 60^o sweep, he found that as the wing span-to-tunnel width ratio increased from 0.175 to 0.35, the wall effects followed similar trends (i.e. vortex breakdown was shifted downstream with increasing wing size). However, when the wing span-to-tunnel width ratio was increased from 0.35 to 0.7, no significant change was observed. This suggested that effective camber was not the only influence. For both the 60^o and the 70^o wings, the difference in breakdown location observed from the smallest model to the largest model, was of the order $25\%c_r$.

Thompson and Nelson[5] investigated experimentally the influence of tunnel walls on a 70^o delta wing by testing full, two thirds, and half scale models in a square tunnel (the largest model gave the ratios S/H = S/W = 0.364). Due to a steady hysteresis effect the wing was tested for a quasi-steady upward and downward stroke. It was found that for the smallest model tested (S/H = S/W = 0.124) the breakdown location shifted downstream by as much as $15\%c_r$ on both the quasi-steady upstroke and downstroke. For the half scale model and the full scale model, there appeared to be little difference in the breakdown locations. As stated by Thompson and Nelson, this shift downstream as model size is decreased is in contrast to the results of Weinberg.[4] It was noted that Weinberg used a Reynolds number an order of magnitude lower, and a constant velocity, as opposed to keeping the Reynolds number constant (as in the experiments of Thompson and Nelson). It was observed that the vortex suction on the model surface increased with model size.

More recently Pelletier and Nelson[6] studied the effect of tunnel interference on 70^o delta wings. Experiments were conducted in a water tunnel with three different sized wings. These low Reynolds number tests agreed with the previous findings of Thompson and Nelson[5] who tested at higher Reynolds number, in that breakdown moved towards the apex with increasing wing size. Pelletier and Nelson used the method of images to explain this effect, concluding that the tunnel walls increased the mean incidence of the wing, thus promoting breakdown.

Verhaagen et al.[7] performed Euler calculations of the flow over a 76^o delta wing inside wind tunnels of increasing size. The wing span-to-tunnel width ratios considered were 0.292, 0.389, and 0.584 and the test section was octagonal. To model the effect of a secondary separation, a small "fence" was placed where secondary separation would occur. It was found that decreasing the tunnel size (increasing the wing span-to-tunnel width ratio) increased the suction in the vortices and increased the velocities in the vortex core, due to an increase in circulation with decreasing tunnel size.

Allan et al.[8] performed Euler simulations of tunnel interference effects on a 65^o delta wing in various tunnels for static and pitching cases. It was observed that tunnel side walls were the most influential factor on breakdown location, with roof and floor having little effect. It was also noted that in pitching simulations, the tunnel interference effects were strongest on the downstroke, during the vortex reformation. It is the aim of this research to confirm the previous Euler results, using the more realistic model of the RANS equations. The solutions of this work are presented.

FLOW SOLVER

All simulations described in this paper were performed using the University of Glasgow PMB3D (Parallel Multi-Block 3D) RANS solver. A full discussion of the code and turbulence models implemented is given in.[9] PMB3D uses a cell centered finite volume technique to solve the Euler and Reynolds Averaged Navier-Stokes (RANS) equations. The diffusive terms are discretised using a central differencing scheme and the convective terms use Roe's scheme with MUSCL interpolation offering third order accuracy. Steady flow calculations proceed in two parts, initially running an explicit scheme to smooth out the flow solution, then switching to an implicit scheme to obtain faster convergence. The pre-conditioning is based on Block Incomplete Lower-Upper (BILU) factorisation and is also decoupled between blocks to help reduce the computational time. The linear system arising at each implicit step is solved using a Generalised Conjugate Gradient (GCG) method. For time-accurate simulations, Jameson's pseudo-time (dual-time stepping) formulation is applied, with the steady state solver used to calculate the flow steady states on each phys-

ical time step (discussed fully in[9]).

Since the RANS equations are solved the 2 equation k-ω model is used for closure. It is well known that most linear 2-equation turbulence models over-predict the eddy viscosity within vortex cores, thus causing too much diffusion of vorticity.[10] This weakens the strength of the vortices and can eliminate secondary vortices, especially at low angles of attack where the vortices are already weak. The following modification suggested by Brandsma et al.[11] was therefore applied to the standard k-ω model of Wilcox[12] to reduce the eddy-viscosity in vortex cores.

$$P_k = min\{P_k^u, (2.0 + 2.0min\{0, r-1\})\rho\beta^* k\omega\} \quad (1)$$

Here P_k^u is the unlimited production of k, P_ω^u is the unlimited production of ω, and r is the ratio of the magnitude of the rate-of-strain and vorticity tensors. When k is over predicted in the vortex core, it will be limited to a value relative to the dissipation in that region. This modification was found to improve predictions compared with the standard k-ω turbulence model[13] and is used in all simulations presented.

The Computational Fluid Dynamics Laboratory at the University of Glasgow owns a cluster of PC's. The cluster is known collectively as Jupiter and is fully described by Badcock et al.[9] There are 32 nodes of 750MHz AMD Athlon Thunderbird uni-processor machines, each with 768Mb of 100MHz DRAM. MPI (Message Passing Interface) is used to link up multiple nodes to create a virtual machine, which is used to execute computationally demanding problems. PMB3D balances the node loadings (number of cells per node) by spreading the blocks over all the nodes of the virtual machine. Halo cell values are passed between adjacent blocks using MPI.

TEST CASES

Computations have been performed on the WEAG-TA15 wing (figure 1). The model consisted of the half wing alone (no body, stings, mountings etc.) inside a square (3x3) tunnel, a 3x2 tunnel, and a 2x3 tunnel (test case details given in table 1). The frontal area blockages for each tunnel were 6.69% for the 2x3 and 3x2 tunnels, and 4.2% for the square tunnel, when the wing is pitched at 21^o. No tunnel contraction or diffuser were modelled since their geometry is unique to a specific tunnel. Inviscid wall conditions were applied at the tunnel wall to reduce the grid sizes required to model the tunnel boundary layers. The WEAG-TA15 wing has

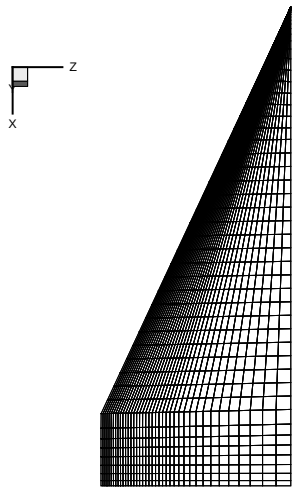

Fig. 1 ***The WEAG-TA15 Wing Surface Mesh (every second point removed for clarity)***

TUNNEL	S/W	S/H	M	Re
SQUARE (3x3)	0.42	0.42	0.2	3.1×10^6
3 X 2	0.42	0.63	0.2	3.1×10^6
2 X 3	0.63	0.42	0.2	3.1×10^6
Expt	-	-	0.12	3.1×10^6

Table 1 Summary of Test Cases

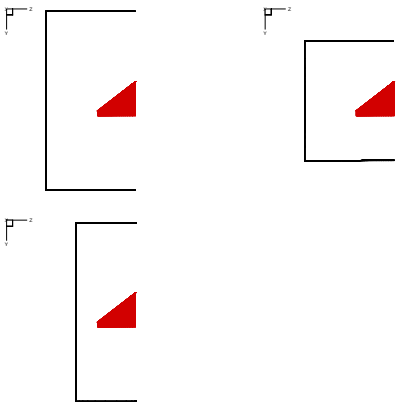

Fig. 2 ***Wind tunnel shapes considered in this study, clockwise from top left, the (a) Square, (b) 3x2, and (c) 2x3 tunnels***

been used in previous simulations[14,15],[8] and these studies have provided a strong foundation for this research.

In order to be able to perform a fair comparison between different tunnels, it was decided that one mesh should be constructed in such a way that removing blocks would allow different tunnel shapes to be assessed. The topology that facilitated this with relative ease was the H-H topology. Views of the wing in the tunnels are shown in figure 2.

There were 320 blocks in the "farfield" mesh

with approximately 4 million grid points. This mesh had the farfield boundary condition applied at 20 c_r lengths from the wing in all directions. Extracting blocks from the farfield mesh gave the different tunnel grids. The square tunnel grid consisted of 80 blocks with approximately 3 million grid points, the 3x2 tunnel grid consisted of 40 blocks with approximately 2,800,000 grid points, and the 2x3 tunnel grid consisted of 56 blocks with 2,600,000 grid points. All three tunnel grids had the farfield condition specified at the inlet, 20 c_r lengths from the wing, with a first order extrapolation boundary at the outlet. Initial cell spacing normal to the wing was $1.0 \times 10^{-6} c_r$ giving $y^+ < 1.0$ over the wing, and the wing was meshed at 21^o.

All pitching computations were at a Reynolds number of 3.1×10^6, a Mach number of 0.2, with a pitching amplitude of 6^o, and a reduced frequency of motion of 0.56. The forcing function used was :

$$\alpha(t) = \alpha_m + \alpha_0 sin(kt)$$

There were 50 time steps per cycle and computations were run until the removal of transient effects (this is usually achieved after 4 complete cycles). A pitching calculation was performed with 100 time steps per cycle at the higher reduced frequency to ensure an adequate temporal resolution. It was concluded that 50 time steps per cycle was sufficient.[13]

VALIDATION

Since the experimental data of Löser[16] was obtained in an open test section wind tunnel, a farfield solution will be used for validation of the steady and pitching solutions. A more accurate validation could be conducted if the pressure distribution around the test section was measured. This pressure distribution could be used as a boundary condition for a more accurate simulation of the open test section.

A comparison of the computed and experimental surface pressures at three chordwise locations is given in figure 3. As can be seen the primary vortex suction levels compare very well with experiment at the chordwise locations of x/c_r=0.3, x/c_r=0.6, and x/c_r=0.8. However, one noticeable difference is the location of the primary vortex core. In the CFD solution the primary vortex core is clearly more inboard than was observed in experiment (most evident at the chordwise locations of x/c_r=0.3 and 0.6). This indicates that the secondary vortex is too large, as a larger secondary vortex will push the primary vortex core inboard[17].[18] It is also clear that the secondary

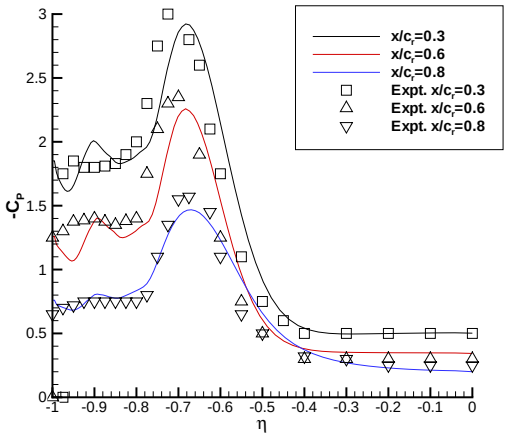

Fig. 3 *Comparison of computed upper surface pressure distributions with experiment*

suction region predicted by CFD is more peaky (again most evident at the chordwise locations of x/c_r=0.3 and 0.6) than that found in experiment. This indicates a stronger secondary flow in the CFD solutions when compared to experiment. The early secondary separation can be attributed to the turbulence levels in the boundary layer predicted by the modified k-ω model (a reduction of turbulence in the boundary layer is understood to cause earlier secondary separation). Interestingly, at the chordwise location of $x/c_r = 0.8$, the primary and secondary suction levels compare very well with experiment, and as such the primary vortex core location is also well predicted. Note that at this chordwise location there is a smaller spanwise pressure gradient (due to the vortices being burst), thus reducing the dependency of the solution on the boundary layer profile. Despite the more inboard primary vortex in the CFD solutions, it is concluded that the flow over the WEAG-TA15 wing has been well predicted.

A limited grid dependency study was presented by Allan.[13] Since an identical resolution of the vortical region is used in all simulations, and grid dependency will be common to all solutions. All simulations were converged four orders of magnitude with the maximum residual being located at the leading edge of the wing.

RESULTS AND DISCUSSION

Steady Results

Before conducting pitching simulations, steady simulations of the wing at 21^o were performed. The breakdown locations for the four WEAG-TA15 wing test cases are given in table 2. Note that no experimental breakdown locations are

TUNNEL	S/W	S/H	Breakdown Location
Farfield	-	-	$77.4\%c_r$
Square	0.42	0.42	$75.7\%c_r$
3x2	0.42	0.63	$75.4\%c_r$
2x3	0.63	0.42	$70.8\%c_r$

Table 2 Summary of steady breakdown locations for WEAG-TA15 wing at 21^o angle of attack

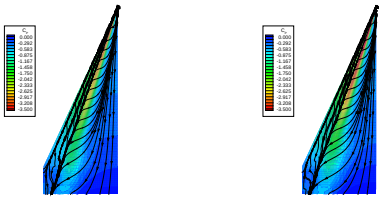

(a) Farfield (b) 2x3 tunnel

Fig. 4 ***Upper surface pressure distributions with shear stress streamlines***

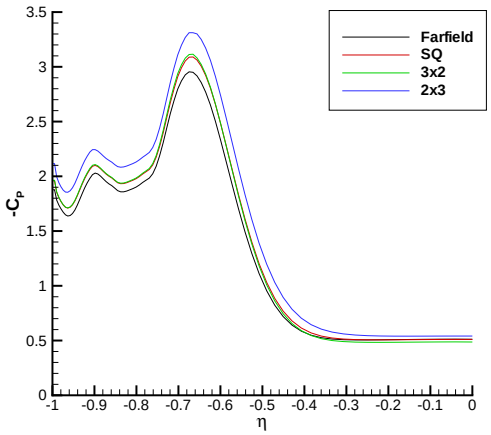

Fig. 5 ***Comparison of upper surface pressure distributions, x/c_r = 0.3***

available.

The breakdown locations were obtained by extracting a vertical slice through the vortex core and finding the point where the axial velocity component becomes negative. As in the results of the Euler simulations of Allan et al.,[8] it can be seen that the trends of breakdown location within tunnel wall constraints predicted by the RANS solver are similar to those predicted by the Euler equations. For the square and 3x2 tunnels it can be seen that the breakdown locations are almost identical, slightly nearer the apex in comparison to the farfield results, indicating that the roof and floor proximity has little influence. Comparing the 2x3 tunnel breakdown locations with those from the square (3x3) and 3x2 tunnels, we clearly see that the largest influence on breakdown location is due to the side wall proximity. This agrees with the Euler results.

Figure 4 shows the upper surface pressure distributions for the farfield and 2x3 tunnel solutions. Upper surface shear stress streamlines have also been shown. The secondary separation and reattachment locations are clearly visible. Between the secondary separation and reattachment lines there is also another set of separation and attachment lines. This is due to a small region of separation just after the secondary vortex core. It is possible that this additional separation may not be present in experiment as it has already been observed that the secondary vortex appears stronger in the CFD solutions, and also that the boundary layer profile may not be as full as in experiment.

A comparison of the upper surface pressure distributions at two chordwise locations is given in figures 5 and 6. As with Euler simulations[8] it is clear that as the wing enters a tunnel, the suction peak beneath the primary vortex core increases. Although not presented here, there is a very minor shift in the secondary separation location towards the leading edge of the wing when in the tunnels. Any delay in secondary separation is likely to be dependent on the upper surface shape (the WEAG-TA15 wing has a convex upper surface), the primary suction peak, and the crossflow momentum. A more apparent shift in secondary separation location was observed in tunnel interference effects on a flat upper surface 70^o delta wing.[19] Inboard of the primary vortices (near the centreline) it can seen that there is additional suction on the wing upper surface due to the blockage effect of the tunnels. Looking closely at the pressure distributions at x/c_r=0.6, the effect of the promotion of vortex breakdown towards the apex can be seen. All the pressure curves become much closer to the pressure distribution from the farfield solution. This is due to vortex breakdown being closer to the x/c_r=0.6 station in the tunnel solutions than in the farfield solution. It is also evident that when the roof and floor are brought closer to the wing there is little change in the suction peak (compare the 3x2 and square tunnel solutions), which indicates that roof and floor proximity has little bearing on the strength of the vortices.

The tunnel wall pressure distributions for all three tunnels are given in figure 7. As in the Euler solutions for these cases, there is a clear favourable pressure gradient in the axial direction. This is expected as the vortices become closer to the side wall as they extend towards the trailing edge of the wing. At the cropped tip of the wing the side wall induced upwash will

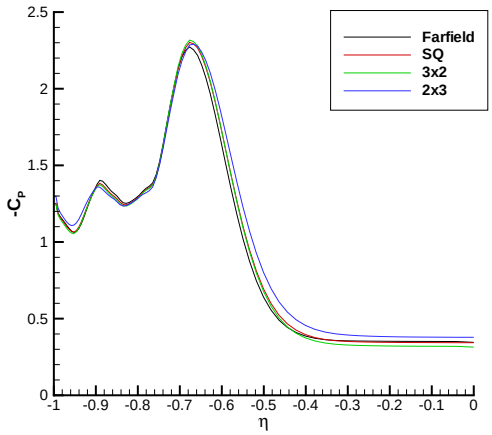

Fig. 6 *Comparison of upper surface pressure distributions, x/c_r = 0.6*

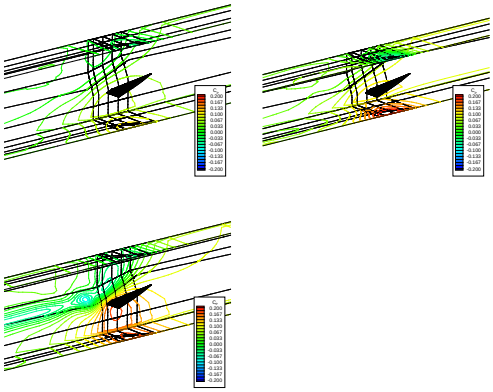

Fig. 7 *Tunnel wall pressure distributions, clockwise from top left, the (a) Square, (b) 3x2, and (c) 2x3 tunnels*

be greatest producing the largest suction on the wall. Looking at the strength of the pressure contours, the pressure gradient on the wall becomes more favourable as the side wall is moved closer to the wing, which is seen as we move from the square to the 2x3 tunnel. Again as seen in Euler solutions there is a clear vortical flow pattern on the side wall downstream of the wing's trailing edge. This vortical flow pattern extends the length of the tunnel. The vortical flow pattern on the side walls is observed for the three tunnels, reducing in extent with decreasing S/W ratio.[20] It is clear that the close proximity of the 2x3 tunnel side wall induces the largest favourable pressure gradient, indicating that the side wall produces the most detrimental interference.

In order to assess the adverse pressure gradient experienced by the vortex core in the tunnels, the pressure distribution along the leading edge

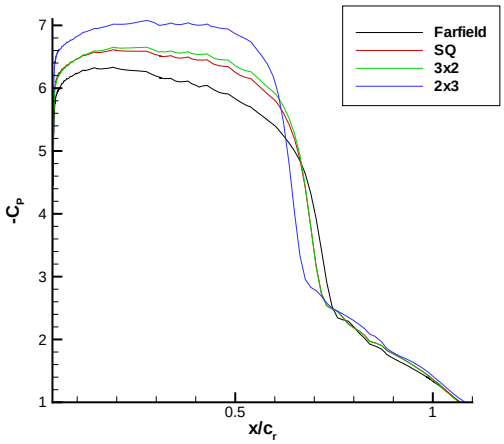

Fig. 8 *Pressure distributions along vortex core*

vortex core is shown in figure 8. As the vortex is placed within tunnel constraints it can be seen that the suction in the vortex core increases, with the largest increment being observed in the 2x3 tunnel. The square and 3x2 tunnels produce a similar increment in suction. This increase induces a stronger adverse pressure gradient as seen in figure 8, thus promoting vortex breakdown.

The flow angles (the angle at which the flow is deflected due to the presence of the wing) at the 2x3 tunnel side wall location are shown in figure 9. As in the Euler results[8] it can be seen that the presence of the side walls has increased the flow angles along the wing, thus increasing the mean effective incidence of the wing. Evidently the proximity of the 2x3 tunnel side wall induces the largest mean incidence, followed by the square and 3x2 tunnels which induce a near equal mean incidence. Clearly it is the presence of the side wall which will influence how much the mean effective incidence changes. The increase in mean effective incidence would appear to be dominant over a possible induced camber effect.

The helix angle of the flow through the vortex core can be seen in figure 10. This data was extracted at a chordwise location of x/c_r=0.6 where breakdown is downstream. The helix angle increases due to the side wall induced velocity components, and clearly the roof and floor (as expected) have little effect. The vortex tightens the most in the 2x3 tunnel, followed by the square and 3x2 tunnels which are near equal. An increase in helix angle is well known to promote vortex breakdown.[21]

The tunnel centreline pressure distributions can be seen in figure 11. As was discussed in the Euler simulations,[8] the side wall induced up-

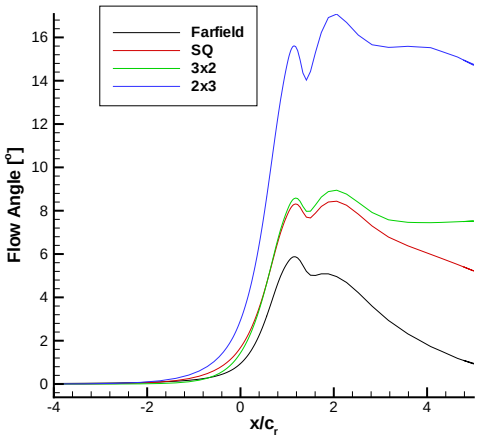

Fig. 9 *Flow angles at 2x3 tunnel side wall location*

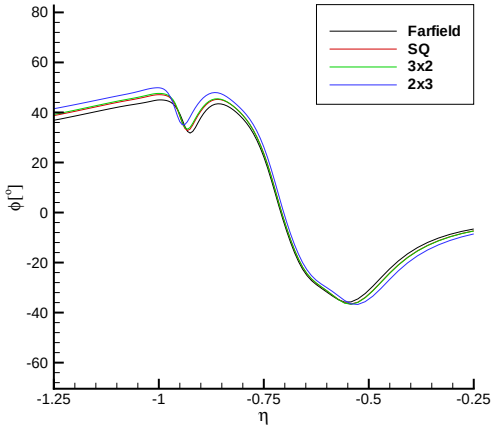

Fig. 10 *Comparison of helix angles,* $x/c_r = 0.6$

wash lifts the vortical system up into the centre of the tunnel. A similar trend is seen with the RANS solutions given in figure 11. It can be seen that the 3x2 and 2x3 tunnels produce similar blockage levels ahead of the wing. The jump from the pressure side to the suction side of the wing can be seen around x/c_r=0.5625. As previously observed, when the wing is placed within tunnel test sections the static pressure increases on the lower surface and decreases on the upper surface due to the blockage effect. As in the Euler solutions, well downstream of the wing the pressure distributions indicate the location of the broken down vortical system. It can seen that the vortical flow in the 2x3 tunnel must be displaced upwards to the centre of the tunnel (this is indicated by a low pressure in comparison to the farfield, square, and 3x2 tunnel solutions). Nearer the trailing edge where the flow on the

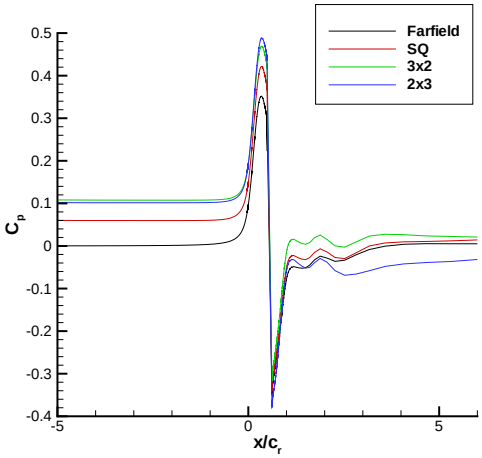

Fig. 11 Tunnel centre line pressure distributions

lower surface is expanding past the trailing edge, the 2x3 tunnel solution exhibits characteristics of the vortical flow being displaced upwards to the centreline of the tunnel. Despite the pressure near the trailing edge being higher than in the farfield solution, one must recall the increment in pressure due to blockage, thus deducting the effect of blockage it is clear the flow near the trailing edge is also lifted off the surface of the wing in comparison to the farfield, square, and 3x2 tunnel solutions. This was confirmed via flow visualisation.

The circulation along the chordwise direction is given in figure 12. The circulation was computed by integrating the axial component of vorticity over entire chordwise slices through the domain. The secondary vortex was eliminated from the calculation of circulation, since the axial vorticity component of the secondary vortex is of opposite sign to that of the primary vortex. Clearly the tunnel walls increase the strength of the vortices in the chordwise direction, with the 2x3 side wall inducing the strongest vortices. The almost equal circulation near the apex, and the steeper gradient of the circulation curve in the tunnels indicates that the effect of the tunnel side walls increases down the leading edge as expected. Since the square and 3x2 tunnels produce similar strength vortices, the roof and floor have little influence on vortex strength.

Pitching results

The lift, drag, and pitching moment curves from each of the pitching cases considered are compared with the experimentally obtained loads and moments in figures 13 to 15. For validation purposes the farfield solution is considered as previously discussed previously. The lift and

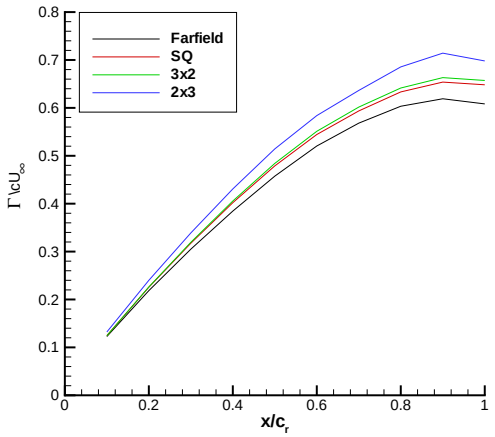

Fig. 12 *Comparison of circulation distributions*

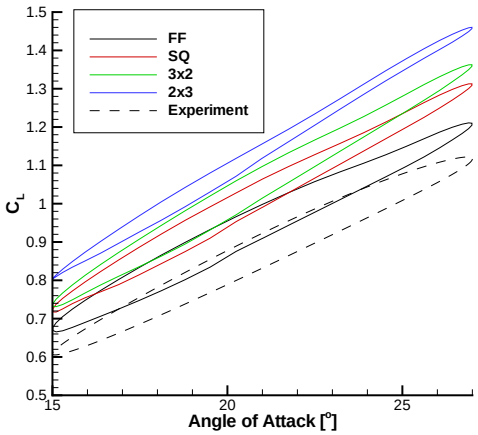

Fig. 13 *WEAG-TA15 wing, $C_L - \alpha$ curves for pitching motion*

drag curves can be seen to have been predicted well, with the lift being slightly over predicted. The magnitude of the pitching moment curves has also been predicted well, though the trend is not so well predicted. However it must be kept in mind that parameters such as pitching moment are very sensitive to vortex breakdown location and vortex strength, which are hard to predict to a high level of accuracy with current RANS methods. As can be seen, particularly in the lift curve, there is a thinning of the hysteresis loop as the angle of attack is increased. This is due to a region of reduced lift curve slope occurring at around 23^o angle of attack. At this incidence it is observed from flow visualisations that vortex breakdown has crossed the trailing edge, resulting in a reduction in the lift curve slope.[22] The resulting non-linearity is not observed in the experimental data which may be a result of the data presentation (the experimental data is given in the frequency domain via Fourier transformation[16]).

Clearly the response of the vortices to pitching motion is predicted sufficiently well and as such comparisons of vortex response to pitching motion in tunnels can be considered.

Considering first the lift and drag curves in figures 13 and 14, we initially see that the tunnels have a considerable influence on the shape and positions of the curves. As the wing is placed into the square tunnel we see an increment of the lift curve. There is also a narrowing of the curve, most evident at the higher incidence. This can be attributed to the vortex breakdown passing the trailing edge at a slightly lower angle of attack when compared with the farfield solution. A similar situation is seen in the 3x2 tunnel where

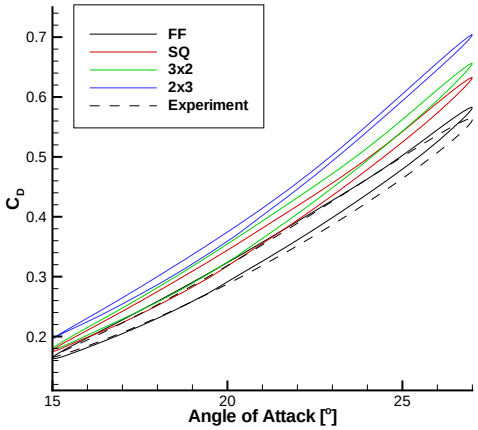

Fig. 14 *WEAG-TA15 wing, $C_D - \alpha$ curves for pitching motion*

the curve is further incremented due to increasing blockage effects. As expected the location at which the lift curve slope drops (when breakdown crosses the trailing edge) appears to be similar in the square and 3x2 tunnels. Finally comparing the 2x3 tunnel solution with that from the farfield solution, we see a further increment in lift as expected with the stronger vortices. Also it is evident that by far the thinnest loops occur for the 2x3 tunnel solution. Again this is due to the fact that vortex breakdown has crossed the trailing edge earliest in the 2x3 tunnel. A similar situation is seen with the drag curves. The thinning of the hysteresis loops can be explained as follows. Since the effect of increasing blockage is to increment the lift and drag, the vortex lift contribution (recalling Polhamus' suction analogy[23]) becomes a lower percentage of the total

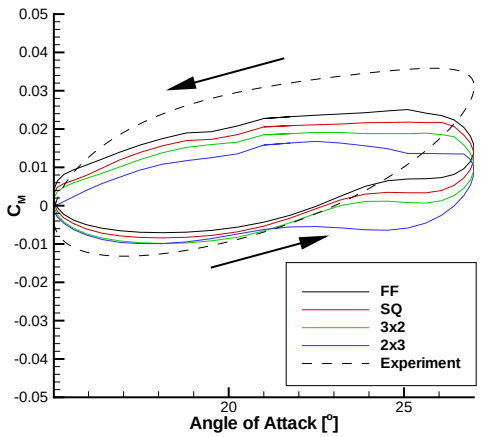

Fig. 15 ***WEAG-TA15 wing,*** $C_M - \alpha$ ***curves for pitching motion***

lift. Therefore when the blockage is increased and the potential lift component becomes larger, the hysteresis due to vortex lift contribution becomes less apparent. If we compare against Euler solutions,[8] where the vortices are closer to the surface and therefore the vortex lift is higher, the effect of the increase in potential lift on the hysteresis is lower. Also since the vortices are closer to the wing in the Euler solutions, an increase in vortex strength (i.e. as incidence or S/W ratio increases) will be more apparent on the suction peaks (and therefore the vortex lift) in comparison to the RANS solutions.

The pitching moment curves provide a good measure of how much the flow structure varies at a given point in the pitching cycle due to tunnel wall constraints. Since breakdown locations are unavailable once breakdown has passed the trailing edge (due to the grid density decreasing in that region), the pitching moment curves provide a great deal of insight as to how the tunnel walls are influencing the flow at the low incidences, being sensitive to longitudinal flow variations. The understanding of the side wall influences on breakdown location gained from the steady results, and the effect that blockage has on the loads and moments, allows a great deal of information to be interpreted solely from the pitching moment curves. Figure 15 shows the pitching moment curves obtained from each solution. Clearly the smallest difference is in the angle of attack region between 15^o to 21^o on the upstroke of the pitching motion. Recalling that the blockage in the 2x3 and 3x2 tunnels is similar (which will have an effect on the pitching moment), it can be concluded that since the pitching moment curves in the 2x3 and 3x2 tunnels are almost identical in the low incidence range, the tunnel side walls have little effect on the vortices. It should also be remembered that wind tunnel wall interference will depend heavily on vortex strength, which increases with incidence (the mirror images strengthen as the leading edge vortices strengthen). Thus we would expect the greatest interference to occur at high incidence. It can therefore be assumed that at low incidence, the difference between the 2x3 and 3x2 tunnel curves, and those from the square and farfield solutions, is purely due to blockage. As the incidence is increased and the influence of the tunnel side walls increases, the effect of the promotion of vortex breakdown crossing the trailing edge early in the 2x3 tunnel can be seen at around 22^o on the upstroke. As the breakdown forms just past the trailing edge there is a slight increase in the nose down pitching moment due to the breakdown region acting like a bluff body in the CFD solutions (a small suction peak is observed on the wing surface beneath the vortex breakdown region). This provides additional suction near the trailing edge increasing the nose down pitching moment slightly. As the incidence increases further and breakdown moves completely onto the wing, a loss of the nose down pitching moment occurs as expected (this occurs earliest in the 2x3 tunnel at around 24.5^o). The solutions from the other two tunnels and the farfield solution follow a similar pattern though this occurs later in the pitching cycle. At around 25^o it is evident that vortex breakdown is well established over the wing in all the solutions (figure 16), which is highlighted by a sharp decrease in the nose down pitching moment. Now considering only the 2x3 tunnel pitching moment curve, it can be seen that from 27^o to around 25^o on the downstroke that the pitching moment remains relatively constant. In this region vortex breakdown is held at its most upstream location (see figure 16 for confirmation) due to the increased influence of the tunnel walls at high incidence, which are promoting vortex breakdown. It can be concluded that as in Euler simulations,[8] there is a delay in vortex recovery. From around 25^o to 22^o it is observed that the 2x3 tunnel solution begins to tend towards that of the other tunnels, which is due to the reducing tunnel interference. From around 22^o downwards it can be seen that the pitching moment curve from all tunnels follow a similar trend to that of the farfield solution as the tunnel inteference lowers. Most attention has been paid to the 2x3 tunnel solution, however, it is also clear that the square and 3x2 tunnels have influenced the curves, both in blockage terms and

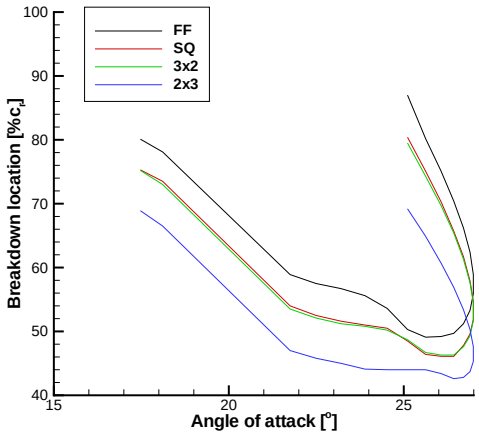

Fig. 16 ***WEAG-TA15 wing, Unsteady breakdown locations for sinusoidal pitching motion***

from a slight promotion of vortex breakdown.

The vortex breakdown locations for the RANS pitching calcs are given in figure 16. Locations at which breakdown is over the wing are only shown. Downstream of the trailing edge the grid coarsens, and as such, breakdown locations cannot be obtained in this region. It should be noted that on the upstroke the vortex breakdown location has been taken where the axial component of velocity becomes zero. However, on the downstroke of the motion where vortex breakdown is moving downstream it is not possible to use this criterion for breakdown, as the motion of the breakdown location prohibits this (the axial velocity does not become zero). As such, for the downstroke the breakdown location was defined as the location where the turbulent Reynolds number (or equally the eddy viscosity) increases rapidly. A turbulence Reynolds number of near 600.0 (where eddy viscosity is 600 times greater than the molecular viscosity) was chosen as the breakdown location which corresponded well with where the axial velocity was observed to become zero on the upstroke. As the wing pitches up the breakdown clearly moves upstream in a near linear manner reaching it's most upstream value at around 26^o on the downstroke. In the 2x3 tunnel in particular it can be seen that the breakdown is held near its most upstream location until around 24^o on the downstroke. Recalling the tendency of the side walls is to promote vortex breakdown, at the high incidence the tendency to promote vortex breakdown is strong therefore breakdown is held upstream. Eventually the tunnel interference begins to lower as the wing pitches down and the breakdown begins to move downstream at a similar rate to

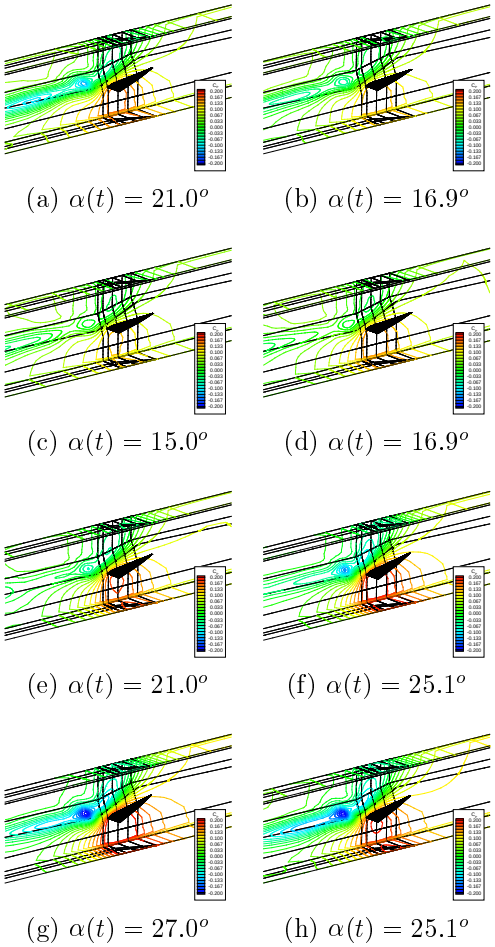

(a) $\alpha(t) = 21.0^o$ (b) $\alpha(t) = 16.9^o$

(c) $\alpha(t) = 15.0^o$ (d) $\alpha(t) = 16.9^o$

(e) $\alpha(t) = 21.0^o$ (f) $\alpha(t) = 25.1^o$

(g) $\alpha(t) = 27.0^o$ (h) $\alpha(t) = 25.1^o$

Fig. 17 ***Sinusoidal pitching, tunnel wall surface pressures within 2x3 tunnel, k = 0.56***

the farfield solution. A similar trend was observed with Euler simulations.[8] It is clear that the initial progression of breakdown downstream is non-linear.[24]

In order to visualise the extent of the interference with incidence the tunnel wall pressure distributions for the 2x3 tunnel are given in figure 17. The side wall interference is clearest in the solutions from the 2x3 tunnel though the discussion applies to the other tunnels. As the wing pitches up and the vortices become stronger we see a much stronger interference pattern on the side walls. It is this strong interference at high incidence which causes the delay in vortex recovery in the 2x3 tunnel. The effect of blockage can also be seen as a high pressure beneath the wing, increasing with frontal area blockage and incidence.

CONCLUDING REMARKS

A study has been conducted to investigate the various effects wind tunnel wall constraints have on delta wing aerodynamics. The following con-

clusions can be drawn from the study :

- The simulations have shown that the RANS equations can adequately model the leeward surface flow over delta wings.
- The simulations have shown that the side walls have the dominant role in wind tunnel interference on delta wings.
- The simulations have shown that the presence of the roof and floor has a lesser influence on vortex breakdown, than that of side walls.
- Side wall proximity promotes vortex breakdown.
- The promotion of vortex breakdown is observed in both steady and unsteady computations, however, for sinusoidal pitching motion, the extent of the breakdown promotion is dependent on the whether the wing is on its upstroke or downstroke.
- Side walls have a strong influence on the rate of vortex breakdown motion, being strongest during the downstroke (vortex recovery), and weaker on the upstroke (breakdown travel towards the apex).

None of the simulations presented in this paper have resolved the frequencies associated with vortex breakdown (helical mode instability). Full time-accurate simulations should therefore be conducted to examine the suitability of "steady" simulations of this highly unsteady flow.

ACKNOWLEDGEMENTS

This work was sponsored a by QinetiQ (formerly DERA Bedford) studentship.

References

[1]Garner, H. C., and Rogers, E. W. E. "Subsonic wind tunnel wall corrections". *AGARDograph 109*, 1966.

[2]Karou, A. "Separated vortex flow over slender wings between side walls - theoretical and experimental investigation". *Report LR-300, Dept. of Aerospace Engineering, Delft University of Technology*, 1980.

[3]Engineering Sciences Data Unit. "Blockage corrections for bluff bodies in confined flows". *Item 80024, London*, 1980.

[4]Weinberg, Z. "Effect of tunnel walls on vortex breakdown location over delta wings". *AIAA Journal*, 30(6), June 1992.

[5]Thompson, S. A., and Nelson, R. C. "Wind tunnel blockage effects on slender wings undergoing large amplitude motions". *AIAA-92-3926*, July 1992.

[6]Pelletier, A., and Nelson, R. C. "Factors influencing vortex breakdown over 70^o delta wings". *AIAA-95-3469-CP*, 1995.

[7]Verhaagen, N. G., Houtman, E. M., and Verhelst, J. M. "A study of wall effect on the flow over a delta wing". *AIAA-96-2389*, 1996.

[8]Allan, M. R., Badcock, K. J., and Richards, B. E. "A CFD Investigation of wind tunnel wall influences on pitching delta wings". *AIAA-2002-2938*, June 2002.

[9]Badcock, K. J., Woodgate, M., Stevenson, K., Richards, B. E., Allan, M., Goura, G. S. L., and Menzies, R. Aerodynamics studies on a Beowulf cluster. In P. Wilders et al., editor, *Parallel Computational Fluid Dynamics Practices and Theory*, pages 39–46, May 2002.

[10]Gordnier, R. E. "Computational study of a turbulent delta-wing flowfield using two-equation turbulence models". *AIAA 96-2076*, 1996.

[11]Brandsma, F. J., Kok, J. C., Dol, H. S., and Elsenaar, A. "Leading edge vortex flow computations and comparison with DNW-HST wind tunnel data". *RTO / AVT Vortex Flow Symposium, Loen, Norway*, 2001.

[12]Wilcox, D. C. "Turbulence modelling for CFD". *DCW Industries, Inc., La Cañada, California*, 1993.

[13]Allan, M. "A CFD Investigation of wind tunnel interference on delta wing aerodynamics". *Ph.D. Thesis, University of Glasgow, Glasgow, UK*, October 2002.

[14]Arthur, M. T., Brandsma, F., Ceresola, N., and Kordulla, W. "Time accurate Euler calculations of vortical flow on a delta wing in pitching motion". *AIAA-99-3110*, 1999.

[15]Woodgate, M., Badcock, K., Richards, B. "Time accurate Euler calculations of vortical flow on a delta wing in rolling motion". *European Congress on Computational Methods in Applied Sciences and Engineering (ECCOMAS 2000)*, September 2000.

[16]Löser, T. "Dynamic force and pressure measurements on an oscillating delta wing at low speeds". *Report IB 129-96/9 DLR Braunschweig*, 1997.

[17]Lowson, M. V. "Visualisation measurements of vortex flows". *J. Aircraft*, 28(5):320–327, 1991.

[18]Jupp, M. L., Coton, F. N., and Green, R. B. "A statistical analysis of the surface pressure distribution on a delta wing". *The Aeronautical Journal*, 103:349–357, July 1999.

[19]Allan, M. R., Badcock, K. J., Barakos, G. N., and Richards, B. E. "Wind tunnel interference effects on a 70^o delta wing". *To appear in proceedings of CEAS Aerospace Aerodynamics Conference, The Royal Aeronautical Society, London, UK.*, 10-12 June 2003.

[20]Hsing, C-C. A., and Lan, C. E. "Low-speed wall interference assessment / correction with vortex flow effect". *J of Aircraft*, 34(2), March - April 1997.

[21]Sarpkaya, T. "On stationary and travelling vortex breakdowns". *J. Fluid Mech.*, 45(3):545–559, 1971.

[22]Hummel, D., and Srinivasan, P. S. "Vortex breakdown effects on the low-speed aerodynamic characteristics of slender delta wings in symmetrical flow". *Journal of the Royal Aeronautical Society*, 71, Technical Notes:319–322, 1967.

[23]Polhamus, E. "Predictions of vortex-lift characteristics by a leading-edge suction analogy". *J. Aircraft*, 8(4):193–199, 1971.

[24]Miau, J. J., Chang, R. C., Chou, J. H., and Lin, C. K. "Nonuniform motion of leading-edge vortex breakdown on ramp pitching delta wings". *AIAA Journal*, 30(7):1691–1702, July 1992.